Measurement of the proton structure function F_2 in ep scattering at HERA

ZEUS Collaboration

August 13, 1993

Abstract

This paper presents our first measurement of the F_2 structure function in neutral-current, deep inelastic scattering using the ZEUS detector at HERA, the ep colliding beam facility at DESY. The data correspond to an integrated luminosity of 24.7 nb^{-1}. Results are presented for data in a range of Q^2 from 10 GeV^2 to 4700 GeV^2 and Bjorken x down to $3.0 \cdot 10^{-4}$. The F_2 structure function increases rapidly as x decreases.

The ZEUS Collaboration

M. Derrick, D. Krakauer, S. Magill, B. Musgrave, J. Repond, S. Repond, R. Stanek, R.L. Talaga, J. Thron
Argonne National Laboratory, Argonne, IL, USA [n]

F. Arzarello, R. Ayad[1], G. Bari, M. Basile, L. Bellagamba, D. Boscherini, A. Bruni, G. Bruni, P. Bruni, G. Cara Romeo, G. Castellini [2], M. Chiarini, L. Cifarelli, F. Cindolo, F. Ciralli, A. Contin, S. D'Auria, C. Del Papa, F. Frasconi, P. Giusti, G. Iacobucci, G. Laurenti, G. Levi, Q. Lin, B. Lisowski, G. Maccarrone, A. Margotti, T. Massam, D. Monaldi, R. Nania, C. Nemoz, F. Palmonari, G. Sartorelli, R. Timellini, Y. Zamora Garcia[1], A. Zichichi
University and INFN Bologna, Bologna, Italy [f]

A. Bargende, J. Crittenden, K. Desch, B. Diekmann, T. Doeker, A. Frey, M. Geerts, G. Geitz, H. Hartmann, D. Haun, K. Heinloth, E. Hilger, H.-P. Jakob, S. Kramarczyk, M. Kückes[3], A. Mass, S. Mengel, J. Mollen, H. Müsch[4], E. Paul, R. Schattevoy, J.-L. Schneider, D. Schramm, R. Wedemeyer
Physikalisches Institut der Universität Bonn, Bonn, Federal Republic of Germany [c]

A. Cassidy, D.G. Cussans[5], N. Dyce, B. Foster, S. George, R. Gilmore, G.P. Heath, H.F. Heath, M. Lancaster, T.J. Llewellyn, C.J.S. Morgado, J.A. O'Mara, R.J. Tapper, S.S. Wilson, R. Yoshida
H.H. Wills Physics Laboratory, University of Bristol, Bristol, U.K. [m]

R.R. Rau
Brookhaven National Laboratory, Upton, L.I., USA [n]

M. Arneodo, M. Schioppa, G. Susinno
Calabria University, Physics Dept.and INFN, Cosenza, Italy [f]

A. Bernstein, A. Caldwell, I. Gialas, J.A. Parsons, S. Ritz, F. Sciulli[6], P.B. Straub, L. Wai, S. Yang
Columbia University, Nevis Labs., Irvington on Hudson, N.Y., USA [o]

P. Borzemski, J. Chwastowski[7], A. Dwuraźny, A. Eskreys, Z. Jakubowski[8], B. Nizioł, K. Piotrzkowski, M. Zachara, L. Zawiejski
Inst. of Nuclear Physics, Cracow, Poland [j]

L. Adamczyk, B. Bednarek, K. Eskreys, K. Jeleń, D. Kisielewska, T. Kowalski, E. Rulikowska-Zarębska, L. Suszycki, J. Zając
Faculty of Physics and Nuclear Techniques, Academy of Mining and Metallurgy, Cracow, Poland [j]

T. Kędzierski, A. Kotański, M. Przybycień
Jagellonian Univ., Dept. of Physics, Cracow, Poland [j]

L.A.T. Bauerdick, U. Behrens, J.K. Bienlein, S. Böttcher, C. Coldewey, A. Dannemann, G. Drews, P. Erhard[9], M. Flasiński[10], I. Fleck, D.J. Gilkinson, R. Gläser[11], P. Göttlicher, B. Gutjahr, T. Haas, L. Hagge, W. Hain, D. Hasell, H. Hultschig, G. Jahnen[12], P. Joos, M. Kasemann, R. Klanner, W. Koch, L. Köpke, U. Kötz, H. Kowalski, W. Kröger, J. Krüger[4], J. Labs, A. Ladage, B. Löhr, M. Löwe, D. Lüke, J. Mainusch, O. Mańczak, M. Momayezi[13], J.S.T. Ng, S. Nickel, D. Notz, K.-U. Pösnecker[14], M. Rohde, J. Roldán[15], E. Ros[7], U. Schneekloth, J. Schroeder, W. Schulz, F. Selonke, E. Stiliaris[15], E. Tscheslog[16], T. Tsurugai, W. Vogel[17], D. Westphal, G. Wolf, C. Youngman
Deutsches Elektronen-Synchrotron DESY, Hamburg, Federal Republic of Germany

H.J. Grabosch, A. Leich, A. Meyer, C. Rethfeldt, S. Schlenstedt
DESY-Zeuthen, Inst. für Hochenergiephysik, Zeuthen, Federal Republic of Germany

G. Barbagli, A. Francescato, M. Nuti, P. Pelfer
University and INFN, Florence, Italy [f]

G. Anzivino, R. Casaccia, S. De Pasquale, S. Qian, L. Votano
INFN, Laboratori Nazionali di Frascati, Frascati, Italy [f]

A. Bamberger, A. Freidhof, T. Poser[8], S. Söldner-Rembold, G. Theisen, T. Trefzger
Physikalisches Institut der Universität Freiburg, Freiburg, Federal Republic of Germany [c]

N.H. Brook, P.J. Bussey, A.T. Doyle, J.R. Forbes, V.A. Jamieson, C. Raine, D.H. Saxon
Dept. of Physics and Astronomy, University of Glasgow, Glasgow, U.K. [m]

H. Brückmann[18], G. Gloth, U. Holm, H. Kammerlocher[8], B. Krebs, T. Neumann, K. Wick
Hamburg University, I. Institute of Exp. Physics, Hamburg, Federal Republic of Germany [c]

A. Fürtjes, E. Lohrmann, J. Milewski[19], M. Nakahata[20], N. Pavel, G. Poelz, W. Schott, J. Terron[15], F. Zetsche
Hamburg University, II. Institute of Exp. Physics, Hamburg, Federal Republic of Germany [c]

T.C. Bacon, R. Beuselinck, I. Butterworth, E. Gallo, V.L. Harris, D.B. Miller, A. Prinias,
J.K. Sedgbeer, A. Vorvolakos, A. Whitfield
Imperial College London, High Energy Nuclear Physics Group, London, U.K. [m]

T. Bienz, H. Kreutzmann, U. Mallik, E. McCliment, M. Roco, M.Z. Wang
University of Iowa, Physics and Astronomy Dept., Iowa City, USA [n]

P. Cloth, D. Filges
Forschungszentrum Jülich, Institut für Kernphysik, Jülich, Federal Republic of Germany

S.H. An, S.M. Hong, C.O. Kim, T.Y. Kim, S.W. Nam, S.K. Park, M.H. Suh, S.H. Yon
Korea University, Seoul, Korea [h]

R. Imlay, S. Kartik, H.-J. Kim, R.R. McNeil, W. Metcalf, V.K. Nadendla
Louisiana State University, Dept. of Physics and Astronomy, Baton Rouge, LA, USA [n]

F. Barreiro[21], G. Cases, L. Hervás[22], L. Labarga[22], J. del Peso, J.F. de Trocóniz[23]
Univer. Autónoma Madrid, Depto de Física Teóríca, Madrid, Spain [l]

F. Ikraiam, J.K. Mayer, G.R. Smith
University of Manitoba, Dept. of Physics, Winnipeg, Manitoba, Canada [a]

F. Corriveau, D.S. Hanna[24], J. Hartmann, L.W. Hung, J.N. Lim, R. Meijer Drees, C. Matthews, J.W. Mitchell[7],
P.M. Patel, L.E. Sinclair, D.G. Stairs, M. St.Laurent, R. Ullmann
McGill University, Dept. of Physics, Montreal, Quebec, Canada [a, b]

G.L. Bashindzhagyan, P.F. Ermolov, L.K. Gladilin, Y.A. Golubkov, V.A. Kuzmin, E.N. Kuznetsov, A.A. Savin,
A.G. Voronin, N.P. Zotov
Moscow State University, Institute of Nuclear Pysics, Moscow, Russia [k]

S. Bentvelsen, M. Botje, A. Dake, J. Engelen, P. de Jong, M. de Kamps, P. Kooijman, A. Kruse, H. van der Lugt,
V. O'Dell, A. Tenner, H. Tiecke, H. Uijterwaal[25], M. Vreeswijk, L. Wiggers, E. de Wolf, R. van Woudenberg
NIKHEF-Amsterdam, Netherlands [i]

B. Bylsma, L.S. Durkin, K. Honscheid, C. Li, T.Y. Ling, K.W. McLean, W.N. Murray, I.H. Park,
T.A. Romanowski[26], R. Seidlein
Ohio State University, Physics Department, Columbus, Ohio, USA [n]

G.A. Blair, A. Byrne, R.J. Cashmore, A.M. Cooper-Sarkar, R.C.E. Devenish, D.M. Gingrich[27], P.M. Hallam-
Baker[7], N. Harnew, T. Khatri, K.R. Long, P. Luffman, I. McArthur, P. Morawitz, J. Nash, S.J.P. Smith[28],
N.C. Roocroft, F.F. Wilson
Department of Physics, University of Oxford, Oxford, U.K. [m]

G. Abbiendi, R. Brugnera, R. Carlin, F. Dal Corso, M. De Giorgi, U. Dosselli, F. Gasparini,
S. Limentani, M. Morandin, M. Posocco, L. Stanco, R. Stroili, C. Voci
Dipartimento di Fisica dell' Universita and INFN, Padova, Italy [f]

J.M. Butterworth, J. Bulmahn, G. Feild, B.Y. Oh[29], J. Whitmore[30]
Pennsylvania State University, Dept. of Physics, University Park, PA, USA [o]

U. Contino, G. D'Agostini, M. Guida[31], M. Iori, S.M. Mari, G. Marini, M. Mattioli, A. Nigro
Dipartimento di Fisica, Univ. 'La Sapienza' and INFN, Rome, Italy [f]

J.C. Hart, N.A. McCubbin, K. Prytz, T.P. Shah, T.L. Short
Rutherford Appleton Laboratory, Chilton, Didcot, Oxon, U.K. [m]

E. Barberis, N. Cartiglia, C. Heusch, B. Hubbard, J. Leslie, W. Lockman, K. O'Shaughnessy, H.F. Sadrozinski, A. Seiden, D. Zer-Zion
University of California, Santa Cruz, CA, USA [n]

E. Badura, J. Biltzinger, R.J. Seifert, A.H. Walenta, G. Zech
Fachbereich Physik der Universität-Gesamthochschule Siegen, Federal Republic of Germany [c]

S. Dagan[32], A. Levy
School of Physics, Tel-Aviv University, Tel Aviv, Israel [e]

T. Hasegawa, M. Hazumi, T. Ishii, S. Kasai[33], M. Kuze, S. Mine, Y. Nagasawa, T. Nagira, M. Nakao, H. Okuno, I. Suzuki, K. Tokushuku, S. Yamada, Y. Yamazaki
Institute for Nuclear Study, University of Tokyo, Tokyo, Japan [g]

M. Chiba, R. Hamatsu, T. Hirose, K. Homma, S. Kitamura, S. Nagayama, Y. Nakamitsu
Tokyo Metropolitan University, Dept. of Physics, Tokyo, Japan [g]

R. Cirio, M. Costa, M.I. Ferrero, L. Lamberti, S. Maselli, C. Peroni, A. Solano, R. Sacchi, A. Staiano
Universita di Torino, Dipartimento di Fisica Sperimentale and INFN, Torino, Italy [f]

M. Dardo
II Faculty of Sciences, Torino University and INFN - Alessandria, Italy [f]

D.C. Bailey, D. Bandyopadhyay, F. Benard, S. Bhadra, M. Brkic, B.D. Burow, F.S. Chlebana, M.B. Crombie, G.F. Hartner, G.M. Levman, J.F. Martin, R.S. Orr, J.D. Prentice, C.R. Sampson, G.G. Stairs, R.J. Teuscher, T.-S. Yoon
University of Toronto, Dept. of Physics, Toronto, Ont., Canada [a]

F.W. Bullock, C.D. Catterall, J.C. Giddings, T.W. Jones, A.M. Khan, J.B. Lane, P.L. Makkar, D. Shaw, J. Shulman
University College London, Physics and Astronomy Dept., London, U.K. [m]

K. Blankenship, J. Kochocki, B. Lu, L.W. Mo
Virginia Polytechnic Inst. and State University, Physics Dept., Blacksburg, VA, USA [o]

K. Charchuła, J. Ciborowski, J. Gajewski, G. Grzelak, M. Kasprzak, M. Krzyżanowski, K. Muchorowski, R.J. Nowak, J.M. Pawlak, A. Stopczyński, T. Tymieniecka, R. Walczak, A.K. Wróblewski, J.A. Zakrzewski, A.F. Żarnecki
Warsaw University, Institute of Experimental Physics, Warsaw, Poland [j]

M. Adamus
Institute for Nuclear Studies, Warsaw, Poland [j]

H. Abramowicz[19], Y. Eisenberg, C. Glasman[34], U. Karshon[32], A. Montag[32], D. Revel, A. Shapira
Weizmann Institute, Nuclear Physics Dept., Rehovot, Israel [d]

C. Foudas, C. Fordham, R.J. Loveless, A. Goussiou, I. Ali, B. Behrens, S. Dasu, D.D. Reeder, W.H. Smith, S. Silverstein
University of Wisconsin, Dept. of Physics, Madison, WI, USA [n]

W.R. Frisken, K.M. Furutani, Y. Iga
York University, Dept. of Physics, North York, Ont., Canada [a]

[1] supported by Worldlab, Lausanne, Switzerland
[2] also at IROE Florence, Italy
[3] now at TRIUMF, Vancouver
[4] now a self-employed consultant
[5] now at Rutherford Appleton Laboratory
[6] now at Univ. of Hamburg on an Alexander von Humboldt Research Award
[7] now at CERN
[8] now at DESY
[9] now at IST GmbH, Darmstadt
[10] on leave from Jagellonian University, Cracow
[11] now at Martin & Associates, Hamburg
[12] now at Harry Hoffmann, Fitzbek
[13] now at Univ. of Minnesota, Minneapolis
[14] now at Lufthansa, Frankfurt
[15] supported by the European Community
[16] now at Integrata, Frankfurt
[17] now at Blohm & Voss, Hamburg
[18] deceased
[19] on leave from Warsaw Univ.
[20] now at Institute for Cosmic Ray Research, University of Tokyo
[21] on leave of absence at DESY, supported by DGICYT
[22] partially supported by Comunidad Autónoma de Madrid, Spain
[23] supported by Fundación Banco Exterior
[24] now at DESY as Alexander von Humboldt Fellow
[25] now at SSC, Dallas
[26] now at Department of Energy, Washington
[27] now at Centre for Subatomic Research, Univ.of Alberta, Canada and TRIUMF, Vancouver, Canada
[28] now with McKinsey Consultants, Sidney, Australia
[29] on leave and supported by DESY 1992-93
[30] on leave and supported by DESY 1993-94
[31] permanent address Dip. di Fisica, Univ. di Salerno, Italy
[32] supported by the MINERVA Gesellschaft für Forschung GmbH
[33] now at Hiroshima National College of Maritime Technology
[34] supported by the DAAD - Deutscher akademischer Austauschdienst

[a] supported by the Natural Sciences and Engineering Research Council of Canada
[b] supported by the FCAR of Quebec, Canada
[c] supported by the German Federal Ministry for Research and Technology (BMFT)
[d] supported by the MINERVA Gesellschaft für Forschung GmbH, by the Israel Ministry of Energy, and by the Israel Academy of Science
[e] supported by the Israel Ministry of Energy, and by the German Israeli Foundation
[f] supported by the Italian National Institute for Nuclear Physics (INFN)
[g] supported by the Japanese Ministry of Education, Science and Culture (the Monbusho) and its grants for Scientific Research
[h] supported by the Korean Ministry of Education and Korea Science and Engineering Foundation
[i] supported by the Netherlands Foundation for Research on Matter (FOM)
[j] supported by the Polish State Committee for Scientific Research (grant No. 204209101)
[k] supported by the German Federal Ministry for Research and Technology (BMFT), the Volkswagen Foundation, and the Deutsche Forschungsgemeinschaft
[l] supported by the Spanish Ministry of Education and Science through funds provided by CICYT
[m] supported by the UK Science and Engineering Research Council
[n] supported by the US Department of Energy
[o] supported by the US National Science Foundation

1 Introduction

Inclusive lepton nucleon scattering experiments have been essential to our present understanding of hadronic substructure. Precise measurements of the deep inelastic scattering of charged [1, 2] and neutral [3] leptons from nucleon and nuclear targets have allowed determinations of the parton distributions [4, 5, 6]. These measurements have provided important tests of Quantum Chromodynamics both from studies of the Q^2 evolution of the structure functions and from comparisons to the predictions of various sum rules. Recent theoretical interest has focused on the behavior of the parton distributions at low values of Bjorken x [7, 8], where nonperturbative effects are expected to become important. It is anticipated that the linear GLAP [9] equations for the evolution of the parton density distributions will have to be replaced by nonlinear equations as the transition between perturbative and nonperturbative regions is approached [7, 10].

Fixed target experiments have been limited to values of $x > 8 \cdot 10^{-3}$ for $Q^2 > 4$ GeV^2 [2]. HERA, with its current center of mass energy of 296 GeV , has allowed the experiments H1 [11] and ZEUS [12] to extend their measurements down to $x \sim 10^{-4}$ at $Q^2 > 10$ GeV^2. It is in this x and Q^2 range that we can begin to test the new theoretical ideas.

We present here the first measurement of the F_2 structure function in neutral current scattering using the ZEUS detector. The data were taken during a two month period in the autumn of 1992, using 26.7 GeV electrons colliding with 820 GeV protons. The data sample corresponds to an integrated luminosity of 24.7 nb^{-1}. Preliminary F_2 measurements from the H1 collaboration have been reported [13].

2 The ZEUS detector and experimental running conditions

The ZEUS detector has been described previously [12, 14]. The detector components used for this analysis were the uranium-scintillator calorimeter (CAL), the central tracking detector (CTD), the beam monitor (C5), the vetowall counters and the luminosity detector (LUMI). The coordinate system, centered on the nominal interaction point, is defined with positive **z** along the direction of the proton beam and positive **y** upwards. The CAL consists of three parts covering different regions of the polar angle θ: forward (FCAL, $2.2° \leq \theta \leq 39.9°$), barrel (BCAL, $36.7° \leq \theta \leq 129.1°$) and rear (RCAL, $128.1° \leq \theta \leq 176.5°$). Each of the parts is subdivided into towers of typically 20 $\times$ 20 cm^2 transverse dimension, which in turn are segmented in depth into electromagnetic (EMC) and hadronic (HAC) sections. The EMC sections are further subdivided transversely into cells of 5 $\times$ 20 cm^2 (10 $\times$ 20 cm^2 for RCAL). Each cell is read out by two photomultiplier tubes, providing redundancy and a position measurement within the cell. A fraction of the RCAL EMC towers were instrumented with a hadron-electron-separator (HES) consisting of 3 $\times$ 3.2 cm^2 silicon diodes located at a depth of 3.3 X_0.

The calorimeter has an energy resolution of $\sigma_E = 0.35\sqrt{E(\mathrm{GeV})}$ for hadrons and $\sigma_E = 0.18\sqrt{E(\mathrm{GeV})}$ for electrons as measured under test beam conditions [15]. The CAL also provides a time resolution, $\lesssim 1$ ns for energy deposits $\gtrsim 4.5$ GeV, which is used in background rejection. The calorimeter noise, which is dominated by the uranium radioactivity, is in the range 15 - 19 MeV for EMC cells and 24 - 30 MeV for HAC cells in different calorimeter parts. A cut of 60 MeV for EMC cells and 110 MeV for HAC cells minimizes the effect of noise on the determination of the kinematic variables.

The CTD is a cylindrical drift chamber consisting of 72 layers organized in nine superlayers. It operates in a solenoidal magnetic field of 1.43 T. Three of the inner superlayers were read out for this data taking period with a z-by-timing readout system [16]. The hit position resolution was 4.5 cm in z and 940 μm in the transverse plane. The C5 beam monitor consists of two small scintillation counters separated by 5 mm of lead that partially surround the beam pipe at the rear of the RCAL. These counters were used to detect backgrounds from interactions of the proton beam upstream of the detector and to measure the timing and longitudinal structure of both the proton and electron beams. The vetowall detector consists of two layers of scintillation counters mounted on either side of an iron wall, located near $\mathbf{z} = -7.3$ m, and was also used to tag background particles.

For the data analyzed here, HERA operated with nine pairs of colliding electron and proton bunches spaced by 96 ns. The spread of the interaction point was $\sigma_{\mathbf{z}} = 25$ cm, dominated by the length of the proton bunch. One additional proton and one additional electron bunch were left unpaired to allow studies of beam-related backgrounds.

The luminosity was determined by a measurement of the rate of hard bremsstrahlung photons produced in the Bethe-Heitler process $e\,p \rightarrow e\,p\,\gamma$. The photons were detected in a lead-scintillator calorimeter placed at $\mathbf{z} = -106$ m. The background rate from electron beam bremsstrahlung on the residual gas in the beampipe was subtracted using the unpaired electron bunch. Measurements of the C5 timing distributions indicated that approximately 12% of the electron current was in satellite bunches, which were shifted with respect to the nominal bunches by 8 ns. Since ep interactions from electrons in these satellite bunches fail the event selection criteria (see Section 5) their contribution of 6.5 % to the measured luminosity was removed. The final integrated luminosity of 24.7 nb^{-1} was determined from the corrected photon rate, the detector acceptance and the known Bethe-Heitler cross section. A systematic error of 5% was assigned for the uncertainty in the subtraction of the electron gas bremsstrahlung and satellite bunch contributions, and the uncertainty in the detector acceptance. The statistical error was negligible.

3 Kinematics at HERA

In deep inelastic scattering (DIS) the structure functions are defined as functions of Bjorken x and Q^2, the negative of the four-momentum transfer squared. In the absence of QED radiation at the electron vertex, the basic quantities are:

$$Q^2 = -q^2 = -(k - k')^2 \tag{1}$$

$$x = \frac{Q^2}{2P \cdot q} \tag{2}$$

$$y = \frac{P \cdot q}{P \cdot k} \tag{3}$$

where k and k' are the four-momenta of the initial and final state electrons, respectively, P is the initial state proton four-momentum, and y is the fractional energy transfer to the proton in its rest frame.

The kinematics can be determined from combinations of the leptonic and hadronic energies and angles. We chose the double-angle (DA) method in this analysis because it is less sensitive to scale errors in the energy measurement of the final state particles [17]. In this method, the event variables (x_{DA}, Q^2_{DA}) are derived from the angle of the final state electron θ_e and the

angle γ_H of a massless object balancing the momentum vector of the electron to satisfy four-momentum conservation. In the naïve quark-parton model γ_H is the scattering angle of the struck quark. It is determined from the hadronic energy flow measured in the detector using the equation

$$\cos\gamma_H = \frac{(\sum_h p_{\rm x})^2 + (\sum_h p_{\rm y})^2 - (\sum_h (E - p_{\rm z}))^2}{(\sum_h p_{\rm x})^2 + (\sum_h p_{\rm y})^2 + (\sum_h (E - p_{\rm z}))^2} \tag{4}$$

where the sums, $\sum_h$, run over all calorimeter cells h which are not assigned to the scattered electron, and $(p_{\rm x}, p_{\rm y}, p_{\rm z})$ is the momentum vector assigned to each cell of energy E. The cell angles are calculated from the geometric center of the cell and the vertex position of the event. For the experimental cuts discussed later, we chose the Jacquet-Blondel [18] estimator of the variable y determined using the equation

$$y_{JB} = \frac{\sum_h (E - p_{\rm z})}{2E_e} \tag{5}$$

where E_e is the electron beam energy.

4 Monte Carlo simulation

Monte Carlo event simulation was used to correct for acceptance and resolution effects. The detector simulation is based on the GEANT [19] program and incorporates our best knowledge of the experimental environment and trigger.

Neutral current DIS events with $Q^2 > 2\,\mathrm{GeV}^2$ were generated using the HERACLES [20] program, which includes first order electroweak radiative corrections. The hadronic final state was simulated using the color-dipole model [21] as implemented in ARIADNE [22] for the QCD cascade, and JETSET [23] for the soft hadronization. To study the sensitivity of resolution and acceptance corrections to fragmentation models, a sample of DIS events was also generated using the HERWIG [24] program for the QCD cascades and soft hadronization. These programs give a reasonable description of our observed hadronic energy flow [25]. For the parametrizations of the parton density distributions we used the MRS D$'_-$ set [6].

The main source of background for DIS events is photoproduction at low Q^2 and high y, where the electron scatters through a small angle but transfers a substantial fraction of its energy to the hadronic final state. A photon or a low energy charged pion may be misidentified as the scattered electron and thus contaminate the DIS sample. To study this effect, we generated events with $Q^2 < 2$ GeV^2 with the PYTHIA [26] program. The spectrum of scattered electrons was generated down to $Q^2 = 0$ using the ALLM parametrization [27] of the total photoproduction cross section. The hadronic final state was simulated in the $\gamma^* p$ center of mass system using the multiparton interaction scheme [28] implemented in PYTHIA for hadron–hadron scattering.

The data sample contains a contribution ($\sim 5\%$) from events with a large rapidity gap in the hadronic final state [29]. These events were not adequately simulated in the above Monte Carlo programs. A separate Monte Carlo calculation [30] was therefore performed in which these events were assumed to originate from diffractive excitation of the virtual photon. From this study it was concluded that the acceptance and resolution effects were comparable to those from DIS events in the QCD Monte Carlo simulation described above.

To determine the acceptance of the trigger and data selection, the Monte Carlo events were passed through a selection procedure identical to that for the data described in the next section.

5 Event selection

For this analysis, we kept events triggered by an energy deposit above a threshold of typically 1 GeV in EMC trigger towers of $20 \times 40\,\mathrm{cm}^2$ in the BCAL or RCAL, except for the inner ring of towers around the RCAL beam pipe, which had a trigger threshold of 10 GeV.

The major background at HERA, which we call beam-gas, is produced by proton interactions with the residual gas in the beam pipe or with the beam pipe itself. The primary event selection criteria are therefore designed to recognize and eliminate events with a beam-gas signature. The main criterion used is the time of signals in the CAL and C5 monitor as compared with the nominal time $t = 0$ for signals from ep interactions [12]. Events with a time measured in the C5 monitor or in the CAL consistent with an interaction upstream of the detector (typical RCAL time, $t_{\mathrm{RCAL}} \approx -10ns$) were vetoed online. In the offline selection we further reduced beam-gas background by requiring $|t_{\mathrm{RCAL}}| < 6$ ns. This cut also removed events from interactions originating from the electron satellite bunches.

A variable used to discriminate between background and neutral current DIS events is

$$\delta = \sum_i (E - p_z) \tag{6}$$

where the sum runs over *all* calorimeter cells i. Neglecting detector resolution effects, fully contained neutral current events have $\delta = 2E_e$. After timing cuts, events from beam-gas interactions which do not have energy deposits in C5 or RCAL will have δ close to zero. Photoproduction events, which typically have the scattered electron remaining in the rear beam pipe, also give δ values significantly lower than $2\,E_e$. We therefore removed all events with $\delta < 25$ GeV [12]. Cuts were also applied to remove cosmic muon events based on the pattern of energy deposits in the calorimeter cells, on calorimeter timing and on tracking information.

The above selections reduced the data sample from a total of $4.2 \cdot 10^6$ recorded triggers to 19850 events.

The final event selection criteria were designed to eliminate backgrounds further and to reject DIS events for which the kinematic variables could not be determined with sufficient accuracy. The key signature for neutral current scattering is the presence of the scattered electron in the detector. The identification of such electrons was based on the transverse and longitudinal shower shape in the calorimeter. To ensure high efficiency and purity, an electron energy of at least 5 GeV was required. Spurious low energy electrons, especially in the forward direction, were removed by requiring that y determined from the electron had to be less than 0.95. Elastic QED Compton events were rejected by examining the energy pattern in the calorimeter. Most of the remaining events due to photoproduction were removed by requiring $\delta > 35\,\mathrm{GeV}$.

Determination of the angles θ_e and γ_H requires a measurement of the vertex position. For the $\mathbf{x}$ and $\mathbf{y}$ coordinates we used the nominal beam position of $\mathbf{x} = \mathbf{y} = 0$. When there were sufficient (≥ 2) well-measured tracks within the CTD tracking volume, they were used to determine the $\mathbf{z}$ coordinate of the vertex. The resolution for such events is $\sigma_{\mathbf{z},tracking} \simeq 4$ cm. For events with no tracking vertex, the calorimeter time measurements were used to determine the $\mathbf{z}$ coordinate of the vertex. Since the length of the electron bunch is small compared to the length of the proton bunch, the timing of particles entering the FCAL near $\theta = 0$ determines the vertex position by the equation $t = -2\,\mathbf{z}_{vertex}/\mathrm{c}$. Figure 1a shows the correlation between the FCAL timing and the $\mathbf{z}$ coordinate of the tracking vertex for events where both were available. The vertex reconstruction efficiency from the FCAL time approaches 100% for $E_{\mathrm{FCAL}} > 5$ GeV. The resolution for the vertex from FCAL timing is $\sigma_{\mathbf{z},timing} \simeq 10\,\mathrm{cm}$. In the final sample, the fraction of events with a tracking vertex was 90.2% and the fraction with only a timing vertex

was 9.3%. In the remaining 0.5% of the events, the **z** coordinate of the vertex was set to zero.

The impact position of the electron on the calorimeter was measured from the EMC cells assigned to the electron. The position was calculated from the energy sharing between the two phototubes which view each cell, as well as the energy sharing between neighboring cells. This algorithm was tuned both on information from the HES silicon diodes and test beam data. Figures 1b and 1c show the difference between the position determined by the RCAL and HES measurements. The typical resolution in both **x** and **y** is 1 cm. The resulting θ_e resolution as determined from Monte Carlo depends on the distance of the electron impact point from the beamline, as seen in figure 1d. When an electron enters the detector near the edge of the beampipe hole ($20 \times 20\,\mathrm{cm}^2$) the energy and position measurements are degraded by the partial loss of the shower. We therefore impose a fiducial cut by rejecting events with the scattered electron impact point inside $|\mathbf{x}|, |\mathbf{y}| < 16$ cm.

Figure 1e shows the resolution in γ_H as a function of the cut applied on y_{JB}. In events where both the hadronic transverse momentum and y_{JB} are small, calorimeter noise and resolution effects can have significant impact on the γ_H calculation. To retain sufficient accuracy in the calculation of the DA variables, we require $y_{JB} > 0.04$.

After these cuts an event sample of 2012 events remained with Q^2 values up to $Q^2_{DA} = 4700$ GeV^2.

6 Data characteristics and background

In this section we discuss the agreement between distributions of the final event sample and the Monte Carlo simulation, and the purity and optimal binning of the events for F_2 analysis. We first discuss the vertex simulation and then compare the final distributions of x_{DA} and Q^2_{DA} in the data and Monte Carlo samples. The binning procedure is explained, followed by the estimation of the residual backgrounds in the chosen bins.

It is important to simulate correctly the vertex distribution in the Monte Carlo program to understand the biases introduced by the trigger and event selection criteria for DIS events. An independent sample of photoproduction data taken with the photoproduction trigger, which has negligible selection bias in the vertex distribution, was used to produce the input distribution for the DIS simulation. Figure 2a shows the good agreement between the reconstructed vertex distributions of the data and the Monte Carlo sample.

Figures 2b and 2c show the x_{DA} and Q^2_{DA} data distributions. These are compared to the DIS simulation. The number of Monte Carlo events has been normalized to the number of data events. There is good overall agreement between the shapes of the data and this simulation, which is used to correct the data. Figure 2d shows the distribution of the final event sample in the (x, Q^2)-plane.

The final event sample was binned in x and Q^2 as given in Table 1. The binning was chosen commensurate with the resolution of the measured quantities. The relative resolution in Q^2_{DA} is 25%, independent of Q^2_{DA}. The relative resolution in x_{DA} varies smoothly with x_{DA}, and is 25% for $x_{DA} = 10^{-2}$, 60% for $x_{DA} = 10^{-3}$, and 80% for $x_{DA} = 5 \cdot 10^{-4}$. For this analysis we rejected bins with large corrections or backgrounds. The correction factors in the remaining bins range from 0.8 to 1.9. A total of 1299 events remained in the selected bins in which F_2 was measured.

The contribution from beam-gas background to the sample was estimated by searching for events that pass the event selection cuts but originate from an unpaired electron or proton bunch. One such event was found from the unpaired electron bunch, corresponding to a back-

ground of 9.7 events in the lowest (x, Q^2) bin.

The background remaining from photoproduction was estimated using events generated with the PYTHIA Monte Carlo program. They were passed through the complete event selection to determine the background in each (x, Q^2) bin. As a consistency check the δ distributions, as predicted by the DIS and photoproduction Monte Carlo simulations, were fitted to the δ distribution of the data. This approach gave photoproduction background values in close agreement with the estimates based on the PYTHIA Monte Carlo sample.

The 1299 events have an estimated total background of 35 events distributed in the x and Q^2 bins as shown in Table 1. The maximum background, of about 20%, occurs in the bin $(x = 8.5 \cdot 10^{-4}, Q^2 = 60\ \mathrm{GeV}^2)$. These backgrounds were subtracted from the bins for the following analysis.

7 Extraction of the Nucleon Structure Function F_2

In the momentum transfer range accessible with our integrated luminosity, the electron-proton interactions are to high accuracy described by the exchange of a virtual photon. In deep inelastic scattering the double differential cross section for virtual photon exchange is given in terms of the structure functions by:

$$\frac{d^2\sigma}{dx\,dQ^2} = \frac{2\pi\alpha^2 Y_+}{xQ^4}\left[F_2(x,Q^2) - \frac{y^2}{Y_+}F_L(x,Q^2)\right](1+\delta_r(x,Q^2)) \tag{7}$$

where F_L is the longitudinal structure function and $Y_+ = 1 + (1-y)^2$. The corrections from radiative effects are given by δ_r. When expressed in terms of x and Q^2 determined at the hadronic vertex, δ_r is to a good approximation independent of the structure function F_2.

The unfolding of the acceptance and migration of the events from the 'true' (x, Q^2) to the reconstructed (x, Q^2) was performed by comparing the distributions from the Monte Carlo and data event samples. This gave a bin-by-bin correction to the input structure function used in the Monte Carlo simulation. In each bin, the fractional contribution due to F_L was calculated from QCD using the MRS D'_- parametrization of the parton densities. The correction factors due to the contribution from F_L are small. Table 1 gives the extracted values of F_2 corrected to the (x, Q^2) values listed in the table, together with corrections due to F_L.

Detailed studies were performed to estimate the systematic errors [31]. The possible uncertainties were classified into several categories: understanding of the photoproduction background, electron energy scale, hadron energy scale, electron position, hadron angle, vertex determination, CAL noise, effects of QED radiation, different structure function parametrizations and different reconstruction and unfolding methods. The systematic errors from each category were added in quadrature. We now discuss the most important of these contributions.

Systematic uncertainties stemming from the photoproduction background were studied using several electron finding algorithms, each with varying sensitivity to the isolation of the electron from the hadronic activity. This becomes important at low x where the current jet is in the rear direction, near the final state electron. Typically, algorithms not requiring isolation of the electron were more efficient at low values of x but suffered from a larger photoproduction background. Appreciable differences in the extracted values of F_2 were only observed in the lowest x bins in each Q^2 bin, where effects of up to 10% were found.

Sensitivity to a possible mismatch between the energy reconstructed from the data and the Monte Carlo simulation was negligible for most bins but reached 20% in the lowest x bins. The

Q^2 GeV^2	Q^2 range	x	x range	Events in bin	Back-ground	F_L corr.	Measured $F_2 \pm$ stat $\pm$ sys
15	10 - 20	$4.2 \cdot 10^{-4}$	$3.0 - 6.0 \cdot 10^{-4}$	159	16$\pm$11	1.032	1.14 $\pm$ 0.11 $\pm$ 0.19
		$8.5 \cdot 10^{-4}$	$6.0 - 12. \cdot 10^{-4}$	202	2 $\pm$ 1	1.006	1.05 $\pm$ 0.08 $\pm$ 0.12
		$1.7 \cdot 10^{-3}$	$1.2 - 2.4 \cdot 10^{-3}$	175	0	1.001	0.80 $\pm$ 0.07 $\pm$ 0.08
30	20 - 40	$4.2 \cdot 10^{-4}$	$3.0 - 6.0 \cdot 10^{-4}$	43	1 $\pm$ 1	1.119	1.80 $\pm$ 0.30 $\pm$ 0.46
		$8.5 \cdot 10^{-4}$	$6.0 - 12. \cdot 10^{-4}$	120	4 $\pm$ 2	1.027	1.52 $\pm$ 0.15 $\pm$ 0.17
		$1.7 \cdot 10^{-3}$	$1.2 - 2.4 \cdot 10^{-3}$	119	0	1.005	1.07 $\pm$ 0.11 $\pm$ 0.09
		$4.9 \cdot 10^{-3}$	$2.4 - 10. \cdot 10^{-3}$	125	0	1.001	0.65 $\pm$ 0.06 $\pm$ 0.20
60	40 - 80	$8.5 \cdot 10^{-4}$	$6.0 - 12. \cdot 10^{-4}$	28	6 $\pm$ 2	1.101	1.15 $\pm$ 0.25 $\pm$ 0.20
		$1.7 \cdot 10^{-3}$	$1.2 - 2.4 \cdot 10^{-3}$	48	3 $\pm$ 2	1.023	1.21 $\pm$ 0.19 $\pm$ 0.09
		$4.9 \cdot 10^{-3}$	$2.4 - 10. \cdot 10^{-3}$	106	0	1.003	0.82 $\pm$ 0.08 $\pm$ 0.06
120	80 - 160	$1.7 \cdot 10^{-3}$	$1.2 - 2.4 \cdot 10^{-3}$	20	1 $\pm$ 1	1.086	1.50 $\pm$ 0.37 $\pm$ 0.34
		$4.9 \cdot 10^{-3}$	$2.4 - 10. \cdot 10^{-3}$	50	1 $\pm$ 1	1.011	0.91 $\pm$ 0.13 $\pm$ 0.05
		$3.2 \cdot 10^{-2}$	$1.0 - 10. \cdot 10^{-2}$	31	0	1.000	0.49 $\pm$ 0.09 $\pm$ 0.12
240	160 - 320	$4.9 \cdot 10^{-3}$	$2.4 - 10. \cdot 10^{-3}$	21	1 $\pm$ 1	1.040	1.05 $\pm$ 0.24 $\pm$ 0.18
		$3.2 \cdot 10^{-2}$	$1.0 - 10. \cdot 10^{-2}$	24	0	1.001	0.53 $\pm$ 0.11 $\pm$ 0.05
480	320 - 640	$3.2 \cdot 10^{-2}$	$1.0 - 10. \cdot 10^{-2}$	18	0	1.004	0.80 $\pm$ 0.20 $\pm$ 0.13
1000	> 640	$3.2 \cdot 10^{-2}$	$1.0 - 10. \cdot 10^{-2}$	10	0	1.016	0.60 $\pm$ 0.19 $\pm$ 0.04

Table 1: *Distributions of events and values of the extracted F_2 structure function. The number of events in the bins prior to corrections is tabulated. The background correction is the sum of the events expected in the bin from all background sources. For each value of F_2 the statistical and systematic errors are given. The overall normalization uncertainty of 7% is not included.*

effect of CAL cell noise was studied by varying the $y_{_{JB}}$ cut and gave up to 10% effects only in the bins with lowest y values, corresponding to the highest x bin in each Q^2 range.

We simulated a possible mismatch between the data and Monte Carlo sample vertex distributions by systematically shifting all vertices in the Monte Carlo sample by the estimated maximum uncertainty of ± 3 cm. The largest changes in F_2, up to 15%, were observed in the lowest x bins in each Q^2 range.

We investigated the systematic errors due to the radiative corrections. The double-angle method combined with the δ cut of 35 GeV, which is equivalent to a 9 GeV cut on the energy of an unobserved photon from initial state radiation, limit the effects of radiative corrections to $\lesssim$10 %. Radiative effects were simulated using the HERACLES program.

Several consistency checks were made. The use of the HERWIG Monte Carlo program as an alternative to ARIADNE for simulating the hadronic final state gave the same values of F_2 within statistical errors. Modifying the electron energy cut, the δ cut and the removal of the electron fiducial cut gave negligible changes in the result. The analysis was redone with different combinations of leptonic and hadronic variables to measure x and Q^2. Different unfolding procedures were also used. Changes in the extracted F_2 structure function were small and well understood.

In addition to the bin-by-bin errors, we assign an overall normalization uncertainty of 7%, of which 5% is from the luminosity determination and 5% is from trigger efficiency and acceptance determination. The final statistical and systematic errors are shown in Table 1. It should be

noted that the size of the systematic errors is largely a result of the limited data statistics.

8 Summary

In figure 3 we plot the structure function F_2 versus x for the five lowest Q^2 bins. The data show a significant rise in F_2 towards lower values of x , increasing typically by more than a factor of two as x decreases from 10^{-2} to the lowest measured value of $4.2 \cdot 10^{-4}$. Also shown in this figure are several structure function expectations. At the lowest Q^2 value the data points lie below the MRS D'_- [6] extrapolations and the predictions of GRV(HO) [4], but above the extrapolations of MRS D'_0 [6] and CTEQ1MS [5]. Figure 4 shows the F_2 structure function as a function of Q^2 for fixed x. The data are in accord with the expected logarithmic violation of scaling.

Acknowledgements

We wish to acknowledge the contribution of the HERA machine staff during the first year of operating this new colliding beam facility. The support of the DESY directorate is greatly appreciated.

References

[1] For recent data from charged lepton scattering experiments see:

Reanalysis of SLAC/MIT data: L.W. Whitlow et al., Phys. Lett. 250B (1990) 193.

BCDMS collaboration (D-target): A.C.Benvenuti et al., Phys. Lett. 237B (1990) 592.

[2] NMC collaboration: P.Amaudruz et al., Phys. Lett. 295B (1992) 159.

[3] For recent data from neutral lepton scattering experiments see:

CCFR collaboration : W.C. Leung et al., Nevis Preprint # 1460, Submitted to Phys. Lett., 1993; P.Z. Quintas et al., Nevis Preprint # 1461, Submitted to Phys. Rev. Lett., 1992.

CDHSW collaboration: P.Berge et al., Z. Phys., C49 (1991) 187.

For a review see:

S.R.Mishra and F.Sciulli, Annu. Rev. Nucl. Part. Sci., 39 (1989) 259.

[4] M. Glück, E. Reya and A. Vogt, Phys. Lett. 306B (1993) 391.

[5] CTEQ collaboration: J. Botts et al., Phys. Lett. 304B (1993) 159.

[6] A.D.Martin, R.G.Roberts and W.J.Stirling, Phys. Lett. 306B (1993) 145.

[7] L.V.Gribov, E.M.Levin and M.G.Ryskin, Phys. Rep 100 (1982) 1.

[8] For reviews see:
J. Bartels, Particle World, Vol. 2, 2(1991)46.

B. Badelek et al., Rev. Mod. Phys. 64 (1992) 927.

[9] V. N. Gribov and L. N. Lipatov,Sov. Journ. Nucl. Phys. 15 (1975) 438, 675.

G. Altarelli and G. Parisi, Nucl. Phys. 126 (1977) 297.

[10] A.H.Mueller and J.Qiu, Nucl. Phys. B268 (1986) 427.

E. Kuraev, L. Lipatov and V. Fadin, Sov. Phys. JETP 45 (1977) 199.

Y. Balitsky and L. Lipatov, Sov. J. Nucl. Phys. 28 (1978) 822.

[11] H1 collaboration: T. Ahmed et al., Phys. Lett. 299B (1993) 385.

[12] ZEUS collaboration: M.Derrick et al.,Phys .Lett. 303B (1993) 183.

[13] M. Erdmann et al., DESY-93-077, Presented at the 28th Rencontre de Moriond, 20 - 27 Mar, 1993.

[14] ZEUS collaboration: M.Derrick et al., Phys. Lett. 293B (1992) 465, ibid. 297B (1992) 404.

[15] A.Andresen et al., Nucl. Inst. and Meth. A309 (1991) 101.

A.Bernstein et al., DESY 93-076, Submitted to Nucl. Inst. and Meth. (1993)

[16] N.Harnew et al., Nucl. Inst. and Meth. A279 (1989) 290.

B. Foster et al., Nucl. Phys. B, Proc. Suppl. B32 (1993) 181.

[17] S. Bentvelsen, J.Engelen and P.Kooijman, Proceedings of the Workshop 'Physics at HERA' vol. 1, DESY (1992), 23.

[18] F. Jacquet and A. Blondel, Proceedings of the study of an ep facility for Europe, DESY 79/48 (1979)391, U. Amaldi ed.

[19] GEANT 3.13: R. Brun et al., CERN DD/EE/84-1 (1987).

[20] HERACLES 4.1: A.Kwiatkowski, H.Spiesberger and H.-J.Möhring, Proc. of Workshop on Physics at HERA vol 3., DESY, (1992), 1294.

A.Kwiatkowski, H.Spiesberger and H.-J.Möhring, Z. Phys. C50 (1991), 165.

[21] B. Andersson et al., Z. Phys. C43 (1989) 625.

[22] ARIADNE 3.1: L.Lönnblad, Comput. Phys. Commun. 71 (1992) 15.

[23] JETSET 6.3: T.Sjöstrand, Comput. Phys. Commun. 39 (1986) 347.

T.Sjöstrand and M.Bengtsson, Comput. Phys. Commun. 43 (1987) 367.

[24] HERWIG 5.6: G.Marchesini et al., Comput. Phys. Commun. 67 (1992) 465.

[25] ZEUS collaboration: M.Derrick et al., Z.Phys. C59 (1993) 231.

[26] PYTHIA 5.6: H.-U. Bengtsson and T. Sjöstrand, Comput. Phys. Commun. 46 (1987) 43.

T. Sjöstrand, Proc. of Workshop on Physics at HERA Vol. 3 (DESY, 1992) 1405.

[27] H.Abramowicz et al., Phys. Lett. 269B (1991) 465.

[28] T. Sjöstrand and M.Zijl, Phys. Rev. D36 (1987) 2019.

[29] ZEUS collaboration: M.Derrick et al., DESY-93-093, submitted to Phys. Lett.

[30] N. N. Nikolaev and B. G. Zakharov, Z. Phys. C53 (1992) 331.

[31] S. Bentvelsen, PhD thesis (University of Amsterdam), 1993.

F. Chlebana, PhD thesis (University of Toronto), 1993.

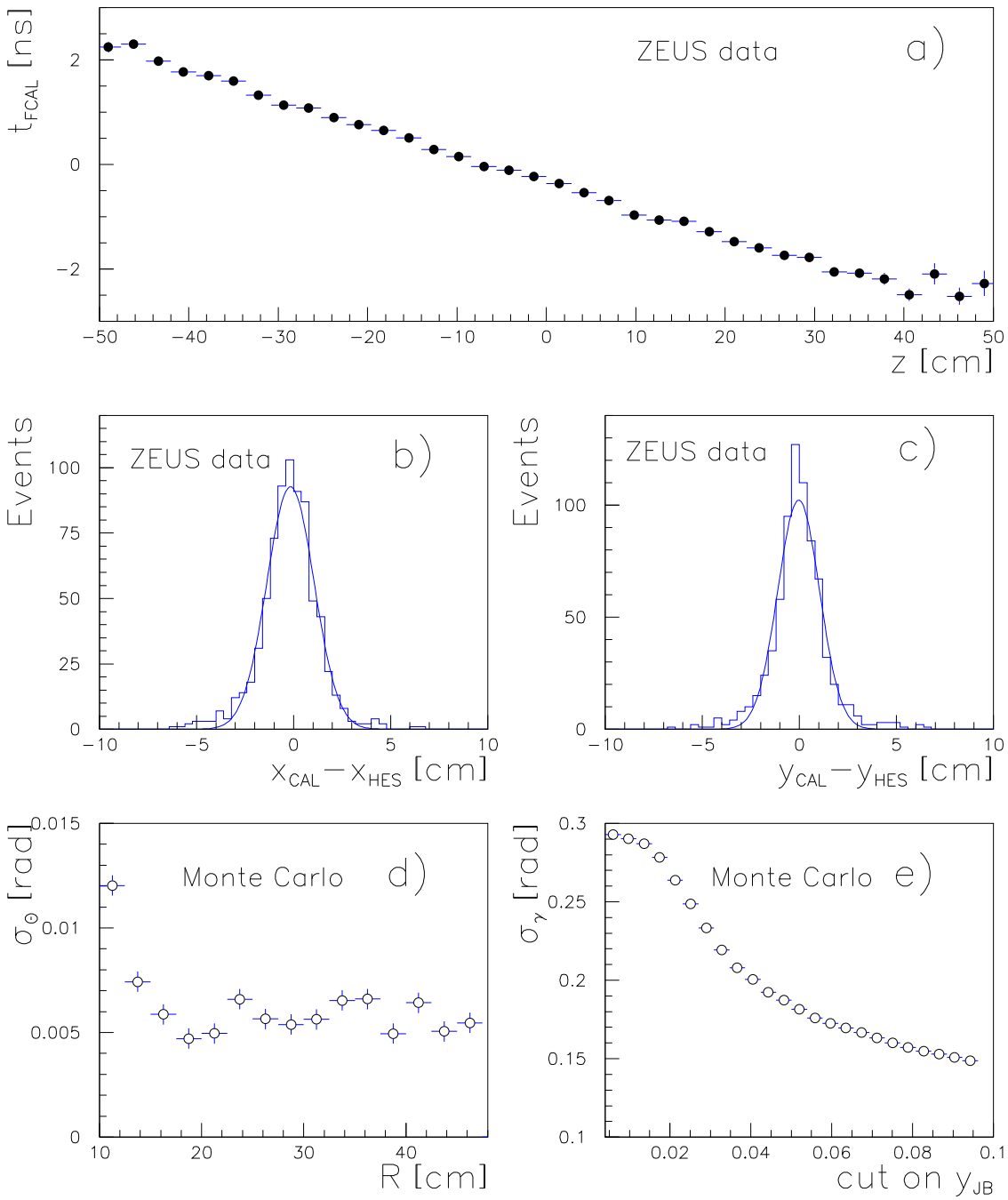

Figure 1: *(a) Correlation between the FCAL time and the* **z** *coordinate of the vertex reconstructed with charged tracks. (b) Difference between the impact* **x***-position of the electron determined from the calorimeter algorithm and from the HES silicon diodes. (c) Same as (b) for the* **y***-position. Note that the HES only covers a limited area of the RCAL. (d) Resolution of the electron angle* θ_e *as a function of the distance,* R*, between the impact point on the RCAL and the beamline. (e) Resolution of the hadronic angle* γ_H *for all events with* y_{JB} *greater than the cut indicated in the figure. Figures (d) and (e) are from Monte Carlo simulations.*

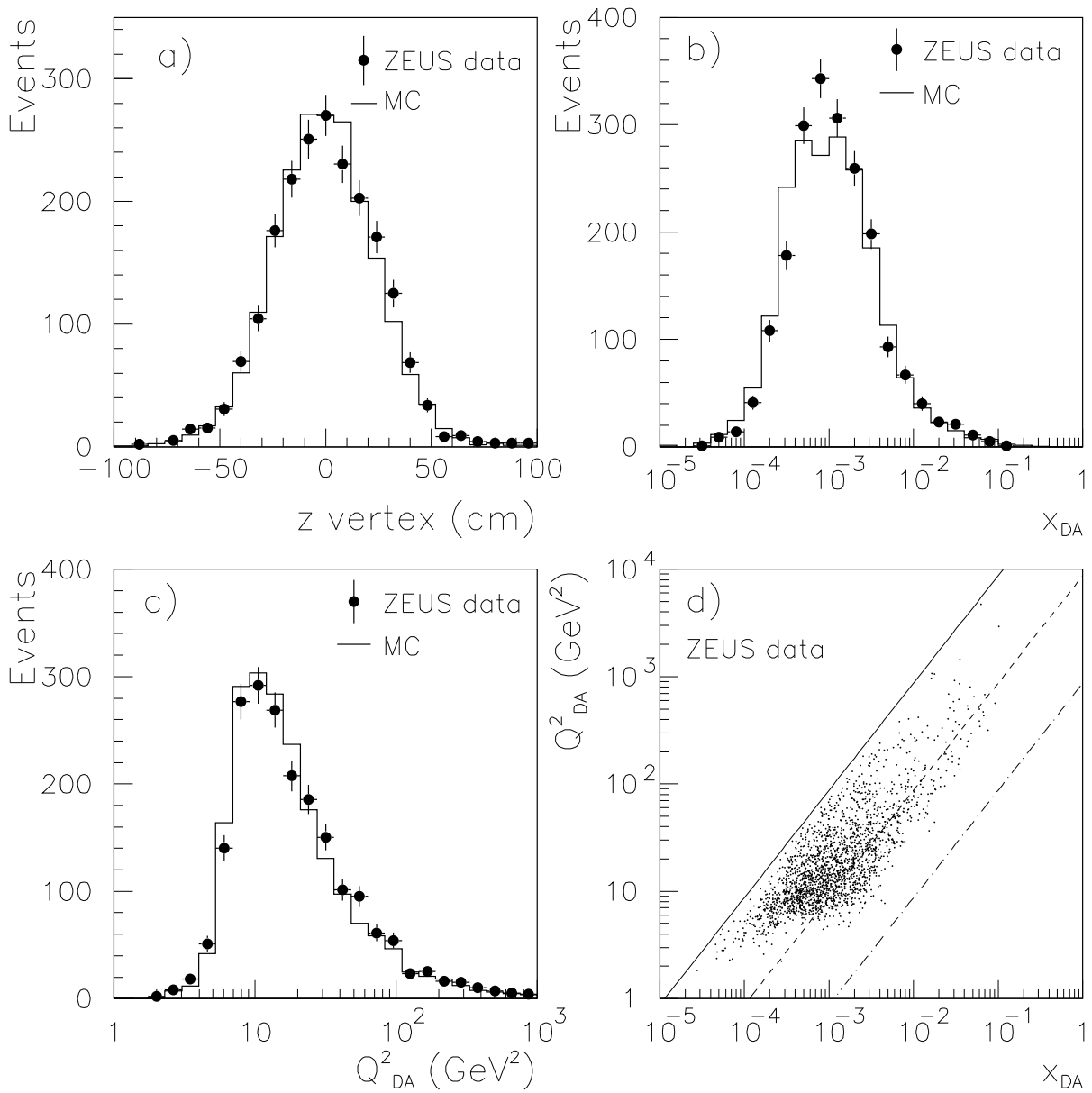

Figure 2: *(a) The reconstructed vertex distributions for data and Monte Carlo event samples. (b) The x_{DA} distribution in the data and Monte Carlo event samples. (c) The Q^2_{DA} distribution in the data and Monte Carlo event samples. In (a), (b) and (c) the number of Monte Carlo events is normalized to the number of data events. (d) Distribution of events in the (x, Q^2) plane; in addition to the kinematic limit $y = 1$ (solid line), the lines $y = 0.1$ (dashed) and $y = 0.01$ (dot-dashed) are drawn.*

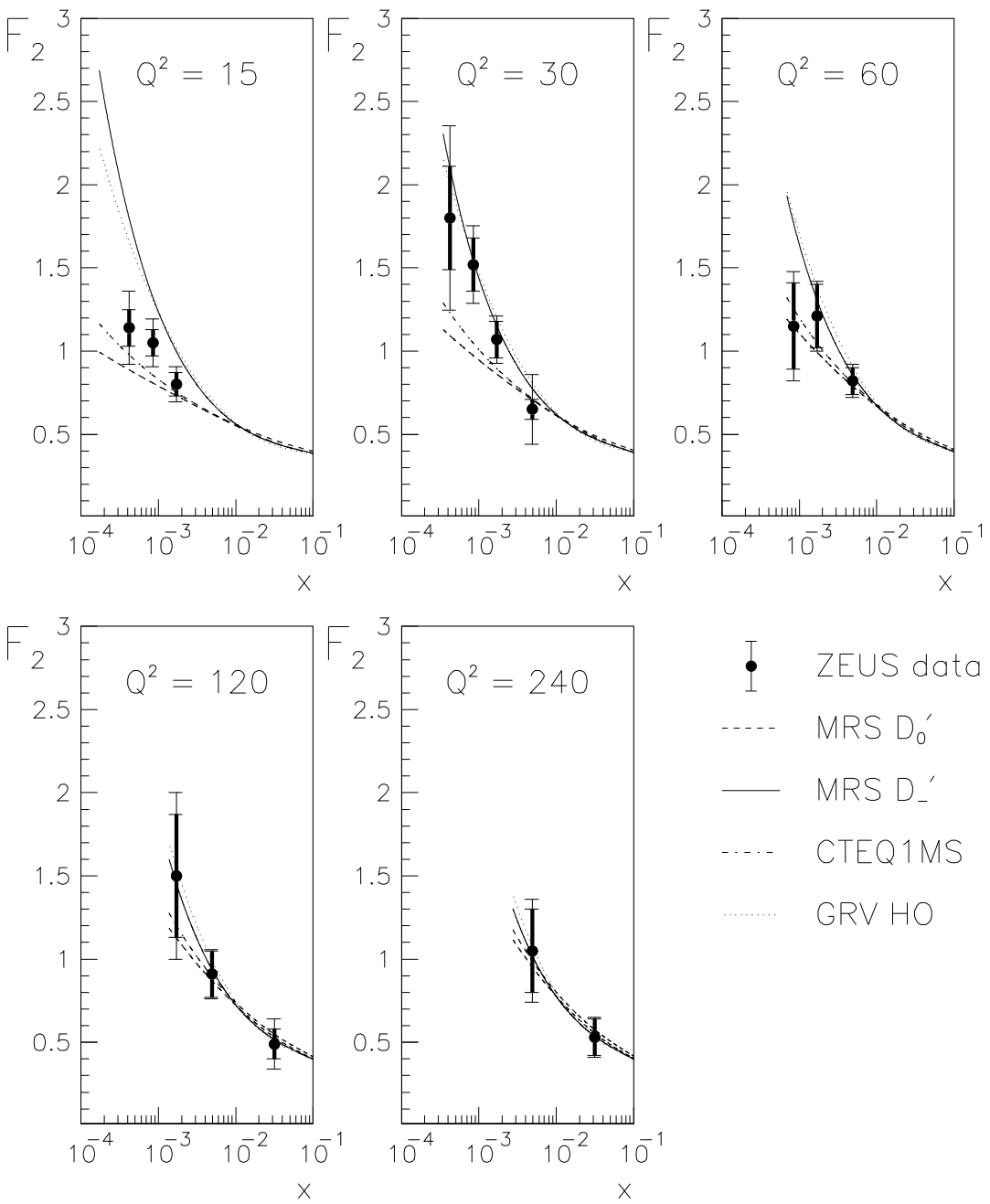

Figure 3: *The structure function F_2 as a function of x for $Q^2 = 15\,GeV^2$, $30\,GeV^2$, $60\,GeV^2$, $120\,GeV^2$ and $240\,GeV^2$. The inner error bar is the statistical error, and the outer bar shows the systematic error added in quadrature. The overall normalization uncertainty of 7 % is not included. In this figure we show only the lowest five Q^2 bins. Also shown are several structure function expectations (all in DIS scheme).*

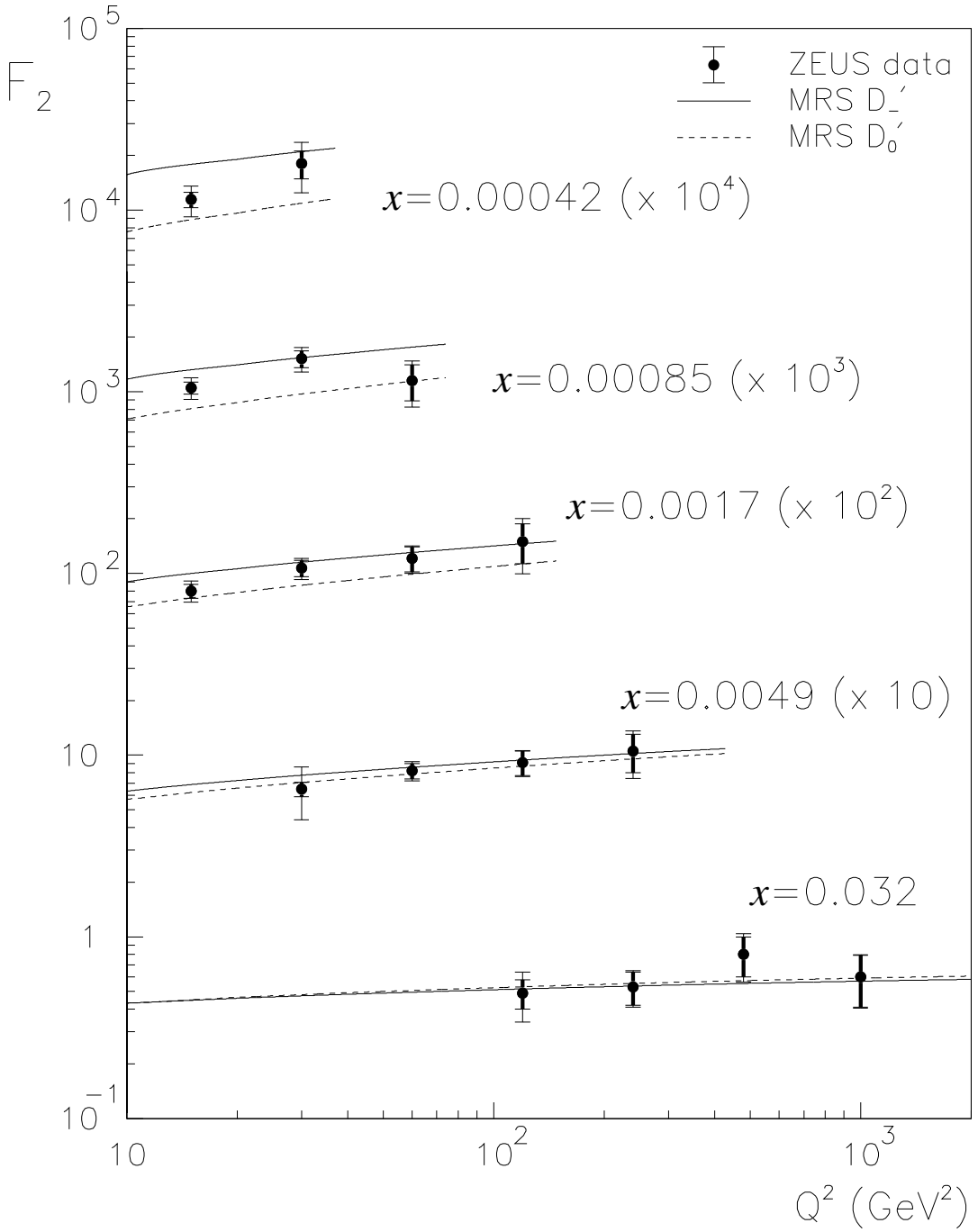

Figure 4: *The structure function F_2 as a function of Q^2 for different values of x. The inner error bar is the statistical error, and the outer bar shows the systematic error added in quadrature. The overall normalization uncertainty of 7 % is not included. Note that the F_2 values are multiplied by different factors (shown in parentheses) for the different x bins. Also shown are two structure function parametrizations.*